Axonal Diameter and Density Estimated with 7-Tesla Hybrid Diffusion Imaging in Transgenic Alzheimer Rats

Madelaine Daianu*[a,b], Russell E. Jacobs [c], Terrence Town[d], Paul M. Thompson[a,b,e]

[a]Imaging Genetics Center, Mark & Mary Stevens Neuroimaging & Informatics Institute, University of Southern California, Marina del Rey, CA, USA
[b]Department of Neurology, UCLA School of Medicine, Los Angeles, CA, USA
[c]Biological Imaging Center, California Institute of Technology, Pasadena, CA
[d]Zilhka Neurogenetic Institute, Keck School of Medicine, University of Southern California, Los Angeles, CA
[e]Departments of Neurology, Psychiatry, Radiology, Engineering, Pediatrics, and Ophthalmology, University of Southern California, Los Angeles, CA, USA

ABSTRACT

Diffusion-weighted MR imaging (DWI) is a powerful tool to study brain tissue microstructure. DWI is sensitive to subtle changes in the white matter (WM), and can provide insight into abnormal brain changes in diseases such as Alzheimer's disease (AD). In this study, we used 7-Tesla hybrid diffusion imaging (HYDI) to scan 3 transgenic rats (line TgF344-AD; that model the full clinico-pathological spectrum of the human disease) *ex vivo* at 10, 15 and 24 months. We acquired 300 DWI volumes across 5 *q*-sampling shells (b=1000, 3000, 4000, 8000, 12000 s/mm^2). From the top three *b*-value shells with highest signal-to-noise ratios, we reconstructed markers of WM disease, including indices of axon density and diameter in the corpus callosum (CC) – directly quantifying processes that occur in AD. As expected, apparent anisotropy progressively decreased with age; there were also decreases in the intra- and extra-axonal MR signal along axons. Axonal diameters were larger in segments of the CC (splenium and body, but not genu), possibly indicating neuritic dystrophy – characterized by enlarged axons and dendrites as previously observed at the ultrastructural level (see Cohen et al., J. Neurosci. 2013). This was further supported by increases in MR signals trapped in glial cells, CSF and possibly other small compartments in WM structures. Finally, tractography detected fewer fibers in the CC at 10 versus 24 months of age. These novel findings offer great potential to provide technical and scientific insight into the biology of brain disease.

Keywords: axonal diameter, multi-shell, HARDI, hybrid diffusion imaging (HYDI), rat, Alzheimer's disease

1. INTRODUCTION

Diffusion-weighted MR imaging (DWI) is sensitive to the organization and geometry of semipermeable barriers within living tissue microstructure [1, 2]. These barriers affect water diffusion in the white matter (WM) and can be picked up in DWI over millisecond timescales [1, 3]. In clinical research, these changes in the WM are most commonly characterized by measures of mean diffusivity and fractional anisotropy (FA) [4] – as reconstructed from the standard diffusion tensors. But although these metrics provide statistics of diffusion anisotropy at voxel level, they do not directly relate to features of tissue microstructure – such as cell size and packing density [1].

Axonal density and diameter are traditionally estimated with invasive histological procedures [e.g., electron microscopy (EM)] and therefore, are limited to *post mortem* tissue. Artifacts may arise from histological procedures (e.g., shrinkage, etc.) and from sampling of small regions of tissue [5]. To overcome some of these limitations, a few DWI-based methods have been proposed to map the axonal density and diameter of the WM matter structure, such as AxCaliber [6] [7], and more recently ActiveAx [1], that models orientation-invariant indices of axonal diameter and density. ActiveAx estimates the MR signal in four compartments of the WM, including intra-, extra-axonal populations of water, stationary water in glial cells and other small structures, and cerebrospinal fluid (CSF) [1].

Here, we implemented the ActiveAx framework and estimated indices of axonal density and diameter in three transgenic Alzheimer rats (line TgF344-AD) at different time points in the disease – 10, 15 and 24 months, using high-field multi-shell imaging, also known as hybrid diffusion imaging (HYDI) [8]. We collected 300 diffusion volumes across 5 distinct *q*-sampling shells and reconstructed the diffusion signal using the diffusion tensor imaging (DTI) model [2] in the corpus callosum (CC). Based on previous EM findings in these transgenic rats [9], we expected to find

Medical Imaging 2016: Image Processing, edited by Martin A. Styner, Elsa D. Angelini, Proc. of SPIE Vol. 9784, 97843G · © 2016 SPIE
CCC code: 1605-7422/16/$18 · doi: 10.1117/12.2216912

indications of dystrophic neurites, or axonal swelling, characterized by enlarged axons and dendrites (possibly filled with vacuoles) as the disease progresses. We provide a summary of axonal density and diameter indices in addition to descriptors of anisotropy and demonstration of tractography based on HYDI, to show altered fiber integrity.

2. METHODS

2.1 Data and Analysis

Three transgenic Alzheimer rats (line TgF344-AD) were generated on a Fischer 344 background by co-injecting rat pronuclei with two human genes driven by the mouse prion promoter: "Swedish" mutant human APP (APPsw) and Δ exon 9 mutant human presenilin-1 (PS1ΔE9) [18]. Transgene integration was confirmed by genotyping and expression levels were evaluated by Western blot of brain homogenates. All experiments were conducted with protocols approved by the Institutional Animal Care and Use Committee (IACUC). The protocol called 'Peripheral TGF-beta Pathway Inhibitor Therapy in Alzheimer's Rats' was approved by the University of Southern California IACUC (Protocol Number: 20044). TgF344-AD rats were housed at the University of Southern California, Zilkha Neurogenetic Institute animal facility. Rats were maintained on normal lab chow and generally housed two per cage, in order to allow socialization. Nesting material was provided to all rats, and environmental enrichment in the form of plastic vertical barriers or tubes was added to all cages. Additionally, extraneous noise that may induce stress was minimized by keeping doors closed to housing rooms. A cage cleaning protocol was adopted that balanced hygiene with the need to retain some odor cues (e.g., scent-marked nesting material) to avoid stress and aggression. Finally, gentle and frequent handling of rats early in life was ensured. Before scanning, we anesthetized the animals with isoflurane, and then performed euthanasia. All efforts were made to minimize suffering.

We scanned the three rats *ex vivo* at 10, 15 and 24 months with a 7 Tesla Bruker BioSpin MRI scanner at the California Institute of Technology. After the three rats were sacrificed at the aforementioned ages, fixed brains (intact within the skull) were soaked in a gadolinium contrast agent (5mM ProHance) for 4 days prior to imaging to decrease the overall T1 of the tissue [10]. To ensure no leakage and that the signal would not change during acquisition, the samples were immersed in galden (perfluoropolyether with same magnetic susceptibility as water). During acquisition, the temperature was monitored via a fiber optic temperature sensor near the sample (and was 20°C for the whole scan) [4].

Using a 3D 8-segment spin echo EPI sequence with 1 average, we acquired 300 DWI volumes (133x233x60 matrix; voxel size: 0.15x0.15x0.25 mm^3; TE=34 ms; TR=500 ms; δ=11 ms; Δ=16 ms), yielding a 20-hour scan time. Specifically, 60 DWI volumes were acquired for each of the 5 *q*-sampling shells, b = 1000, 3000, 4000, 8000 and 12000 s/mm^2, with the same angular sampling, and 5 T2-weighted volumes with no diffusion sensitization (b_0 images). The relatively long δ and Δ values were required to achieve the largest *b*-values within the duty cycle constraints of our gradient coils. This long scan time precludes in vivo imaging, but this is not an issue for fixed samples [11].

During preprocessing, extra-cerebral tissue was removed using the "skull-stripping" Brain Extraction Tool from BrainSuite (http://brainsuite.org/) for both the anatomical images and the DWIs. We corrected for eddy current distortions using the "eddy correct FSL" tool (www.fmrib.ox.ac.uk/fsl) for which a gradient table was calculated to account for the distortions. DWIs were up-sampled to the resolution of the anatomical images (with isotropic voxels) using FSL's flirt function with 9 degrees of freedom; the gradient direction tables were rotated accordingly after each linear registration.

We calculated the signal-to-noise (SNR) ratio of each *q*-sampling shell by computing the average diffusion signal in the WM structure of each rat and estimated noise from the mean standard deviation of all 5 b=0 s/mm^2 images. Then, we ran a 2-tailed *t*-test to determine which *b*-value weighting provided the highest SNR.

2.2 Axonal Diameter Estimation

We modeled four tissue compartments in the WM defined based on the population of water molecules as outlined in [1]. Each compartment provided a separated normalized MR signal: (1) S_1 – signal trapped in the intra-axonal parallel cylinders of equal diameter, a, modeled with the Gaussian phase distribution approximation [12]; (2) S_2 – signal found in the extra-axonal water near but outside the cylinders modeled based on the diffusion tensor (DT) scheme, also assuming Gaussian distributed displacements [2]; (3) S_3 – signal found in the stationary water (S_4 =1 as signal is unattenuated by

diffusion weighting) that may be trapped in glial cells and other subcellular structures (4) S_4 – signal from the CSF; here, the cylinders did not influence the diffusion and the model is isotropic Gaussian displacements [1].

The equation modeled by ActiveAx assumes that no exchange takes place between the compartments of water molecules described above [1]:

$$S^* = S_0^* \sum_{i=1}^{4} f_i S_i \quad (\mathbf{1})$$

Here, S^* is the MR diffusion signal, S_0^* is the MR diffusion signal from the b_0 image, f_1 defines the proportion of water molecules in a population, i, where: $\sum_{i=1}^{4} f_i = 1$ and $0 \le f_i \le 1$.

The axonal diameter was estimated from the following model: $E(a) = \int p(a) a \, da$, where $E(a)$ is the mean axonal diameter and p is the true distribution of axon diameters [1]. For more specifics on the model, please refer to [1]. We assessed the axonal diameter indices at three different segments of the CC – the splenium, body and genu. In this work, we studied the CC as it has larger axonal radii, especially in the middle segment (the body), which can be feasibly reconstructed using the ActiveAx method. In addition, the CC does not have crossing fibers where models like DTI might fail to accurately reconstruct the intersecting fibers at voxel level.

3. RESULTS

To start, we show that the diffusion signal SNR is significantly higher in the lower b-value shells when comparing single- and multi-shell reconstructions between b=1000, 3000 and 4000 s/mm^2 and b=8000 and 12000 s/mm^2 (P=0.03, 2-tailed t-test) (**Fig. 1**). Therefore, we selected the lower 3-shell HYDI data to reconstruct the axonal density and diameter indices.

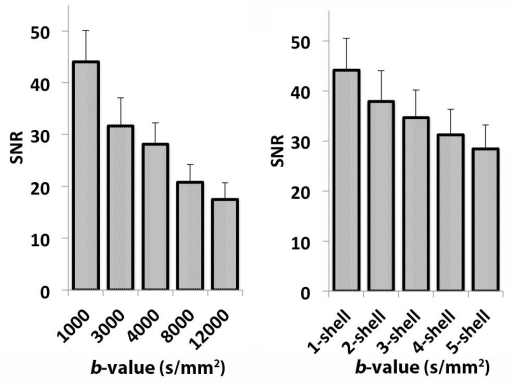

Figure 1. Signal-to-noise ratio (SNR) computed from the diffusion signal in the single b-value DWIs and the multi-shell HYDIs.

For each transgenic Alzheimer rat, we show patterns of alteration directly related to their tissue microstructure (summarized in **Figs. 2** and **3**). The MR signal quantified by the intra- and extra-axonal volume fraction (F1 and F2) decreased with disease progression (at the later stages of disease, 15 and 24 months), possibly indicating less directional water diffusion. This is closely related to decreases in FA; once again indicating altered anisotropic properties of the white matter tissue. The increase in the stationary water volume fraction (F3) and CSF volume fraction (F4) are further suggestive of the etiology of brain tissue disruptions noted on EM [9] in the transgenic Alzheimer rats (e.g., axonal swelling). Increases in F3 could indicate that more water is being trapped within glial cells and other small compartments that are modeled independently of the cylinder-like structures (i.e., modeling the axons).

In accord with our hypothesis, axonal radii were larger in the body of the CC than in the splenium and genu (**Fig. 3A**). Larger axons contain more water and contribute more to the MR signal. With disease progression, axonal radii increased in the splenium and body of the CC, but in the genu they showed opposing patterns; axonal radii in the genu

were also harder to map, so additional studies are needed to confirm these findings. Finally, from our fiber tract maps we show visible decreases in fiber density between the 10 and 24 month old transgenic Alzheimer rats (**Fig. 3B**).

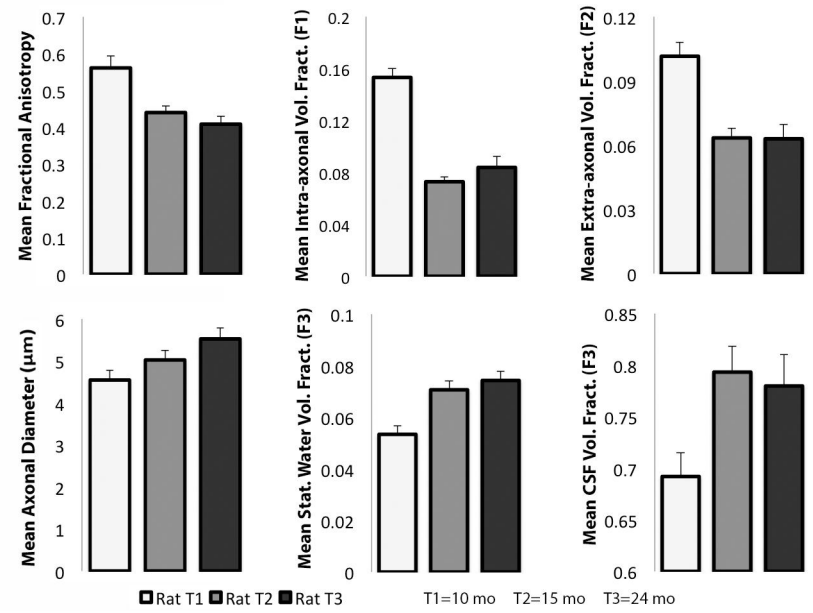

Figure 2. Plots of mean axonal density and anisotropy in the corpus callosum in each transgenic Alzheimer rat. Mean fractional anisotropy (FA) decreased in concordance with decreases in the intra- and extra-axonal volume fraction (F1 and F2). Stationary water and CSF volume fractions (F3 and F4) showed increasing patterns in the later stages of the disease.

4. NEW OR BREAKTHROUGH WORK BEING PRESENTED

In this study, we mapped and interpreted neuroimaging indices directly associated with WM microstructure in transgenic Alzheimer rats at three stages of the disease. To do this, we computed HYDI-based indices of axonal density and diameter and interpreted the observed patterns of disruption in relation to the previously investigated etiology of AD in a recent EM ultrastructural study using TgF344-AD rats [9]. For the first time, we show overlapping findings of altered WM structure going beyond the commonly reported apparent anisotropy changes in AD.

5. CONCLUSION

The involvement of the CC in AD is quite well understood, and the parietal, temporal and possibly occipital segments are among the first affected. Here, we show patterns of decreasing anisotropy in the CC and indices that may contribute to this phenomenon – decreasing intra- and extra-axonal volume fractions. Meanwhile, we also show patterns of increasing stationary water volume fraction that may influence the larger axonal radii observed at the later stages of the disease. Furthermore, increased CSF volume fractions could be explained by atrophy or tissue loss, and are also supported by the lower fiber density in the 24 month old transgenic Alzheimer rat. In this preliminary study we do not have the necessary number of subjects to detect statistically significant differences in the changes observed in the WM microstructure, but the landscape of disruption aligns with changes expected from EM in the cortex and hippocampus in this same transgenic Alzheimer rat line [9].

Understanding the network of WM pathways that supports communication in the brain is critically important to detecting and eventually preventing disease. Measures of axonal density and diameter are important morphological properties of WM, as their integrity is directly related to the rate of information transfer of a nerve bundle and can provide insight into the effects of neurological disease [5], otherwise not detectable with macroscopic neuroimaging metrics. The benefits of HYDI and detailed microscopic indices may be valuable for human [13-16] and animal connectome (**Fig. 3C**) projects and clinical research [4, 17, 18].

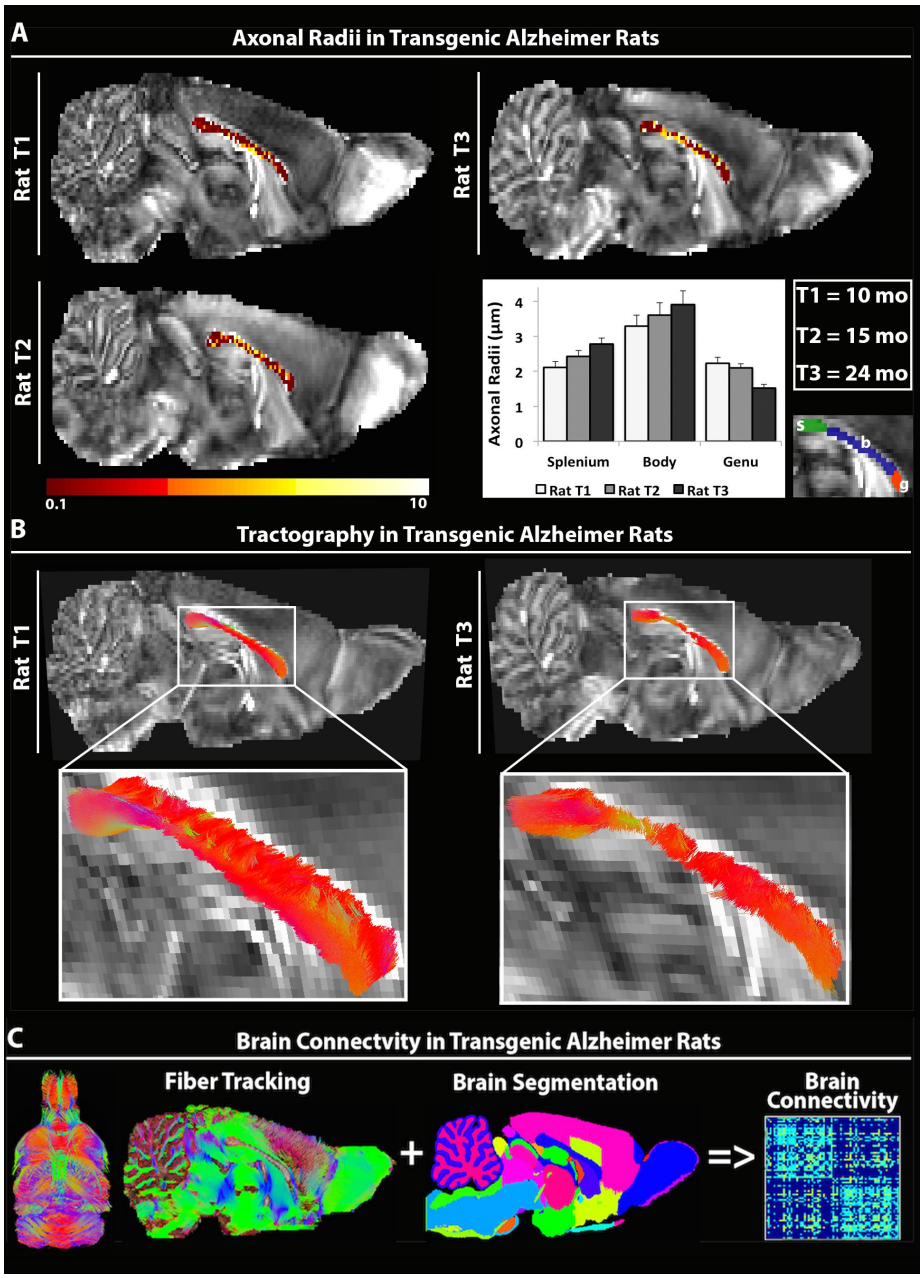

Figure 3. Maps of axonal diameter and fiber density in three transgenic Alzheimer rats. **A.** Axonal diameter indices were evaluated in the splenium, body and genu of the corpus callosum (CC) across the different stages of the disease. As expected, the axonal diameter was larger in the body of the CC than in the splenium and genu. With disease progression, axonal radii increased in the splenium and body of the CC (but not in the genu) - possibly signs of dystrophic neurites and axonal swelling found in electron microscopy studies in these TgF344-AD rats. **B.** Fiber density maps in the CC of the 10 vs. 24 month old rats indicated loss of fibers with disease progression. **C.** For our future work, we aim to reconstruct whole brain connectivity maps using the fiber density maps as depicted in **B**.

Acknowledgments

Algorithm development and image analysis for this study were funded, in part, by grants to PT from the NIBIB (R01 EB008281, R01 EB008432) and by the NIA, NIBIB, NIMH, and the National Library of Medicine (AG016570, AG040060, EB01651, MH097268, LM05639 to PT) and by an NINDS grant to TT (R01 NS076794). Data collection and sharing for this project was funded by NIH Grant R01 AG034499-05. NIBIB & the Beckman Institute at Caltech provided essential support for the scanner & personnel (NIBIB EB000993). TT and TMW were supported by an NIH/NINDS grant (5R01NS076794-05). This work was also supported in part by a Consortium grant (U54 EB020403) from the NIH Institutes contributing to the Big Data to Knowledge (BD2K) Initiative and R01 EB008432.

REFERENCES

[1] D. C. Alexander, P. L. Hubbard, M. G. Hall *et al.*, "Orientationally invariant indices of axon diameter and density from diffusion MRI," Neuroimage, 52(4), 1374-89 (2010).

[2] P. Basser, J. Mattiello, and D. LeBihan, "MR Diffusion Tensor Spectroscopy and Imaging," Biophysical Journal 66, 259-267 (1994).

[3] M. Daianu, M. F. Mendez, V. G. Baboyan *et al.*, "An advanced white matter tract analysis in frontotemporal dementia and early-onset Alzheimer's disease," Brain Imaging and Behavior, In Press (2015).

[4] M. Daianu, R. E. Jacobs, T. M. Weitz *et al.*, "Multi-Shell Hybrid Diffusion Imaging (HYDI) at 7 Tesla in TgF344-AD Transgenic Alzheimer Rats," PLoS One, 10(12), e0145205 (2015).

[5] D. Barazany, P. J. Basser, and Y. Assaf, "In vivo measurement of axon diameter distribution in the corpus callosum of rat brain," Brain, 132(Pt 5), 1210-20 (2009).

[6] Y. Assaf, T. Blumenfeld-Katzir, Y. Yovel *et al.*, "AxCaliber: a method for measuring axon diameter distribution from diffusion MRI," Magn Reson Med, 59(6), 1347-54 (2008).

[7] D. C. Alexander, "A general framework for experiment design in diffusion MRI and its application in measuring direct tissue-microstructure features," Magn Reson Med, 60(2), 439-48 (2008).

[8] M. Daianu, N. Jahanshad, J. E. Villalon-Reina *et al.*, "7T multi-shell Hybrid Diffusion Imaging (HYDI) for mapping brain connectivity in Mice," The International Society for Optics and Photonics (SPIE), Medical Imaging 2015: Image Processing, 9413, 941309-941309 (2015).

[9] R. M. Cohen, K. Rezai-Zadeh, T. M. Weitz *et al.*, "A transgenic Alzheimer rat with plaques, tau pathology, behavioral impairment, oligomeric AB, and frank neuronal loss," Journal of Neuroscience, 33(15), 6245-6256 (2013).

[10] H. Benveniste, K. Kim, L. Zhang *et al.*, "Magnetic resonance microscopy of the C57BL mouse brain," Neuroimage, 11(6 Pt 1), 601-11 (2000).

[11] O. I. Alomair, I. M. Brereton, M. T. Smith *et al.*, "In vivo high angular resolution diffusion-weighted imaging of mouse brain at 16.4 Tesla," PLoS One, 10(6), e0130133 (2015).

[12] J. S. Murday, and R. M. Cotts, "Self-Diffusion Coefficient of Liquid Lithium," The Journal of Chemical Physics, 48(11), 4938 (1968).

[13] M. Daianu, N. Jahanshad, T. M. Nir *et al.*, "Rich club analysis in the Alzheimer's disease connectome reveals a relatively undisturbed structural core network," Human Brain Mapping, 36(8), 3087–3103 (2015).

[14] M. Daianu, A. Mezher, M. F. Mendez *et al.*, "Disrupted rich club network in behavioral variant frontotemporal dementia and early-onset Alzheimer's disease," Hum Brain Mapp, (2015).

[15] M. Daianu, N. Jahanshad, T. M. Nir *et al.*, "Algebraic connectivity of brain networks shows patterns of segregation leading to reduced network robustness in Alzheimer's disease," Medical Image Computing and Computer Assisted Intervention (MICCAI), Computational Diffusion MRI: Springer, 55-64 (2014).

[16] M. Daianu, E. L. Dennis, N. Jahanshad *et al.*, "Alzheimer's disease disrupts rich club organization in brain connectivity networks," IEEE International Symposium of Biomedical Imaging (ISBI), 266-269 (2013).

[17] M. F. Mendez, A. Joshi, M. Daianu *et al.*, "White Matter Changes Associated with Resting Sympathetic Tone in Frontotemporal Dementia vs. Alzheimer's Disease," PLoS One, 10(11), e0142445 (2015).

[18] F. F. Roussotte, M. Daianu, N. Jahanshad *et al.*, "Neuroimaging and genetic risk for Alzheimer's disease and addiction-related degenerative brain disorders," Brain Imaging Behav, 8(2), 217-33 (2014).